

5-31-1991

A new approach to motion analysis from a sequence of stereo images

Lin Zhou
New Jersey Institute of Technology

Follow this and additional works at: <https://digitalcommons.njit.edu/theses>



Part of the [Electrical and Electronics Commons](#)

Recommended Citation

Zhou, Lin, "A new approach to motion analysis from a sequence of stereo images" (1991). *Theses*. 2690.
<https://digitalcommons.njit.edu/theses/2690>

This Thesis is brought to you for free and open access by the Electronic Theses and Dissertations at Digital Commons @ NJIT. It has been accepted for inclusion in Theses by an authorized administrator of Digital Commons @ NJIT. For more information, please contact digitalcommons@njit.edu.

Copyright Warning & Restrictions

The copyright law of the United States (Title 17, United States Code) governs the making of photocopies or other reproductions of copyrighted material.

Under certain conditions specified in the law, libraries and archives are authorized to furnish a photocopy or other reproduction. One of these specified conditions is that the photocopy or reproduction is not to be “used for any purpose other than private study, scholarship, or research.” If a user makes a request for, or later uses, a photocopy or reproduction for purposes in excess of “fair use” that user may be liable for copyright infringement,

This institution reserves the right to refuse to accept a copying order if, in its judgment, fulfillment of the order would involve violation of copyright law.

Please Note: The author retains the copyright while the New Jersey Institute of Technology reserves the right to distribute this thesis or dissertation

Printing note: If you do not wish to print this page, then select “Pages from: first page # to: last page #” on the print dialog screen

The Van Houten library has removed some of the personal information and all signatures from the approval page and biographical sketches of theses and dissertations in order to protect the identity of NJIT graduates and faculty.

21
**A New Approach to Motion Analysis from
a Sequence of Stereo Images**

by
1) LIN ZHOU
/

Thesis submitted to the Faculty of the the Graduate School of
the New Jersey Institute of Technology in partial fulfillment of
the requirements for the degree of
Master of Science in Electrical Engineering
1991

Approval Sheet

Title of Thesis: **A New Approach to Motion Analysis from
a Sequence of Stereo Images**

Name of Candidate: Lin Zhou
 Master of Science in Electrical Engineering, 1991

Thesis & Abstract Approved
by the Examining Committee:

Dr. Yun Qing Shi, Advisor
Assistant Professor
Department of Electrical and Computer Engineering

Date

Dr. Zoran Siveski
Assistant Professor
Department of Electrical and Computer Engineering

Date

Dr. Chang Qing Shu
Research Associate
Department of Electrical and Computer Engineering

Date

New Jersey Institute of Technology, Newark, New Jersey.

Dedicated to
My parents,
My elder brother,
and My wife.

Contents

1	Introduction	1
2	The Optical Flow Approach	3
2.1	Brightness invariance equation and smoothness constraints	3
2.2	Estimating the partial derivatives	4
2.3	Estimating the Laplacian of flow velocities	6
2.4	Minimization	6
2.5	Iterative algorithm	7
3	The Unified Optical Flow Flow Field Approach	9
3.1	Imaging geometry	9
3.2	Four-frame model	14
3.3	Unified optical flow field	15
3.4	A set of equations for analysis of 3-D motion field	16
4	A Simulation Process	20
4.1	Setting	20
4.2	Simulation	24
4.3	Analytic solution	29
4.4	Comparison	33
5	Conclusion and Discussion	40

List of Figures

2.1	Estimation of the three partial derivatives	5
3.1	Imaging geometry	10
3.2	The focal plane of the left camera	12
3.3	Four frame model	14
4.1	Setting	21
4.2	The rotatable sphere	22
4.3	Perspective projection	23
4.4	The four images	25
4.5	The sample pixels	35
4.6	The table of results (size 32*32)	36
4.7	The table of results (size 128*128)	38

VITA

LIN ZHOU

Date of Birth:

Place of birth:

Education:

1989-1991	New Jersey Institute of Technology MSEE
-----------	--

1978-1982	Anshan Institute of Technology, P.R.China BSEE
-----------	---

ACKNOWLEDGMENT

I wish to express my sincere gratitude to Dr. Yun Qing Shi for his valuable guidance, inspiration and encouragement during the entire course of this thesis. I would like to thank Dr. Chang Qing Shu for his valuable guidance. Special thank is extended to Mr. Jingning Pan for his previous work and great assistance. Without their supports, the thesis could not have been finished.

I would also like to thank all people who gave me lots of guidances and suggestions in many ways.

ABSTRACT

Title of Thesis: A New Approach to Motion Analysis from a Sequence of Stereo Images

Author: Lin Zhou

Thesis Directed by: Dr. Yun Qing Shi

A new approach to motion analysis from a sequence of stereo images is presented in this thesis. Based on a four-frame model, a new concept of unified optical flow field has been developed recently [3]. It is a generalization of the optical flow in stereo imagery. A set of fundamental equations is established to characterize the unified optical flow field. Another set of equations is then derived from which 3-D motion can be reconstructed via the use of the field quantities of the unified optical flow field. In this thesis, the implementation of the approach is conducted. The simulation and the results are presented to demonstrate the feasibility and efficiency of this approach.

Chapter 1

Introduction

Over the last ten years, estimation of motion and structure from image sequences has come to play a dominant role within the computer vision community. There are basically two different approaches to recovering the structure of objects and the relative motion between object and cameras: 1) the feature based approach and 2) the optical flow based approach [1].

The feature based approach requires that correspondence be established between a sparse set of features extracted from one image with those extracted from the next image in the sequence. Although several methods have been discussed for extracting and establishing feature correspondence, the task is difficult and only partial solutions suitable for simplistic situations have been developed [1].

The optical flow techniques rely on local spatial and temporal derivatives of image brightness values. And optical flow is the distribution of apparent velocities of movement of brightness patterns in an image [2].

Optical flow can arise from relative motion of objects and the viewer. Consequently, optical flow can give important information about the spatial arrangement of the objects viewed and the rate of change of this arrangement. The optical flow cannot be computed at a point in the image independently of neighboring points without introducing additional constraints, because the velocity

field at each image point in the image plane due to motion yields only one constraint [2].

In Chapter 2, we will further discuss the optical flow method and will derive the equations for determining the velocities of movement of brightness in the images.

In Chapter 3, a newly developed technique to motion analysis from a stereo image sequence is presented [3]. Firstly, "temporal" optical flow field is computed by using the equations introduced in Chapter 2. Secondly, the inherent relation between a pair of stereo images obtained at the same moment is analyzed to establish a "spatial" optical flow field. Thirdly, combining these two types of optical flow fields, a unified temporal-spatial optical flow field is obtained. The word "temporal-spatial" is omitted thereafter for the sake of simplicity. Finally, a set of equations from which 3-D motion field can be reconstructed is derived based on this unified optical flow field. In consequence, 3-D motion, both position and velocity, caused by the relative motion between objects and cameras can be determined from the given sequence of stereo images. It is noted that the recovered 3-D motion is for a whole continuous moving field instead of only for some features. Furthermore, this technique does not require feature correspondence and is hence expected to be much more efficient.

In Chapter 4, a detailed simulation process illustrates the algorithm developed in Chapter 3. Simulation results show the feasibility of the new approach.

Finally, we draw conclusions and discuss some issues in Chapter 5.

Chapter 2

The Optical Flow Approach

Optical flow cannot be computed locally at a point since only one independent measurement is available from the image sequence, while the flow velocity has two components. A second constraint is therefore needed. A method for finding the optical flow pattern is presented which assumes that the apparent velocity of the brightness pattern varies smoothly almost everywhere in the image [2].

2.1 Brightness invariant equation and smoothness constraints

The equation that relates the change in image brightness at a point to the motion of the brightness pattern is established by Horn and Schunck [2]. Let the image brightness at a point (x, y) in the image plane at time t be denoted by $E(x, y, t)$. The brightness of a particular point in the pattern is assumed constant, i.e.,

$$\frac{\partial E}{\partial t} = 0.$$

Using the chain rule for differentiation we have

$$\frac{\partial E}{\partial x} \frac{dx}{dt} + \frac{\partial E}{\partial y} \frac{dy}{dt} + \frac{\partial E}{\partial t} = 0.$$

If we let

$$u = \frac{\Delta dx}{dt} \quad \text{and} \quad v = \frac{\Delta dy}{dt},$$

then we have a single linear equation in the two unknowns u and v ,

$$E_x u + E_y v + E_t = 0,$$

where we have also introduced the additional abbreviations E_x , E_y , and E_t , for the partial derivatives of image brightness with respect to x , y , and t , respectively:

$$E_x = \frac{\Delta \partial E}{\partial x}, \quad E_y = \frac{\Delta \partial E}{\partial y}, \quad E_t = \frac{\Delta \partial E}{\partial t}.$$

However, the flow velocity at point (x, y) cannot be solved from the above equation without introducing additional constraints. The additional constraint proposed by Horn and Schunck [2] and used now popularly in practice is to minimize the square of the magnitude of the gradient of optical flow velocity:

$$\left(\frac{\partial u}{\partial x}\right)^2 + \left(\frac{\partial u}{\partial y}\right)^2 \quad \text{and} \quad \left(\frac{\partial v}{\partial x}\right)^2 + \left(\frac{\partial v}{\partial y}\right)^2.$$

We will use the square of the magnitude of the gradient as smoothness measure.

2.2 Estimating the partial derivatives

We must estimate the derivatives of brightness from the discrete set of image brightness measurements that are available. It is important that the estimates of E_x ,

E_x , and E_t be consistent. That is, they should all refer to the same point in the image at the same time.

We will use a set of eight pixels to estimate E_x , E_y , and E_t at the center of a cube formed by these eight measurements. The relationship in space and time between these measurements is shown in Fig. 2.1

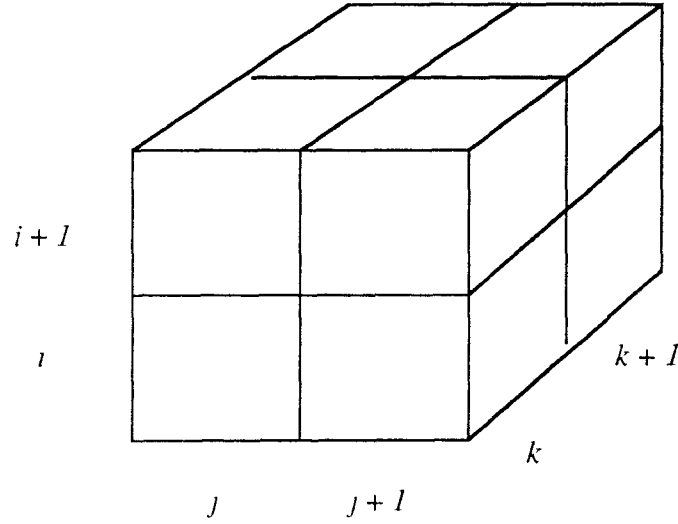


Fig. 2.1. Estimation of the three partial derivatives

Each of the estimates is the average of four first order differences taken over adjacent measurement in the cube.

$$E_x \approx 1/4 \{ E_{i,j+1,k} - E_{i,j,k} + E_{i+1,j+1,k} - E_{i+1,j,k} \\ + E_{i,j+1,k+1} - E_{i,j,k+1} + E_{i+1,j+1,k+1} - E_{i+1,j,k+1} \},$$

$$E_y \approx 1/4 \{ E_{i+1,j,k} - E_{i,j,k} + E_{i+1,j+1,k} - E_{i,j+1,k} \\ + E_{i+1,j,k+1} - E_{i,j,k+1} + E_{i+1,j+1,k+1} - E_{i,j+1,k+1} \},$$

$$E_t \approx 1/4 \{ E_{t+1,j,k} - E_{t,j,k} + E_{t+1,j,k+1} - E_{t+1,j,k} \\ + E_{t,j,k+1} - E_{t,j+1,k} + E_{t+1,j+1,k+1} - E_{t+1,j+1,k} \}.$$

Here the unit of length is the grid spacing interval in each image frame and the time interval is the image frame sampling period.

2.3 Estimating the Laplacian of flow velocities

We also need to approximate the Laplacians of u and v . One convenient approximation assumes the following form

$$\nabla^2 u = *u_{i,j,k} - u_{i,j,k} \quad \text{and} \quad \nabla^2 v = *v_{i,j,k} - v_{i,j,k},$$

where the local averages $*u$ and $*v$ are defined as follows

$$*u_{i,j,k} = 1/6 \{ u_{i-1,j,k} + u_{i,j+1,k} + u_{i+1,j,k} + u_{i,j-1,k} \} \\ + 1/12 \{ u_{i-1,j-1,k} + u_{i+1,j-1,k} + u_{i+1,j+1,k} + u_{i-1,j+1,k} \}, \\ *v_{i,j,k} = 1/6 \{ v_{i-1,j,k} + v_{i,j+1,k} + v_{i+1,j,k} + v_{i,j-1,k} \} \\ + 1/12 \{ v_{i-1,j-1,k} + v_{i+1,j-1,k} + v_{i+1,j+1,k} + v_{i-1,j+1,k} \}$$

2.4 Minimization

A minimization method has been formulated by Horn and Schunck in [2] to determine optical flow. The problem then is to minimize the sum of the errors in the equation for the rate of change of image brightness,

$$\mathcal{E}_b = E_x u + E_y v + E_t,$$

and the measure of the departure from smoothness in the velocity flow,

$$\mathcal{E}_c^2 = \left(\frac{\partial u}{\partial x} \right)^2 + \left(\frac{\partial u}{\partial y} \right)^2 + \left(\frac{\partial v}{\partial x} \right)^2 + \left(\frac{\partial v}{\partial y} \right)^2.$$

Let the total error to be minimized be

$$\mathcal{E}^2 = \iint (\alpha^2 \mathcal{E}_c^2 + \mathcal{E}_b^2) dx dy,$$

where α is used to denote a suitable weighting factor.

The minimization is to be accomplished by finding suitable values for the optical flow velocity (u, v) . Using the calculus of variation one can obtain

$$E_x^2 u + E_x E_y v = \alpha^2 \nabla^2 u - E_x E_t,$$

$$E_x E_y u + E_y^2 v = \alpha^2 \nabla^2 v - E_y E_t.$$

Using the approximation to the Laplacian introduced in the previous sub-section, and solving the set of linear equations for u and v , one can find out

$$(\alpha^2 + E_x^2 + E_y^2)(u - *u) = -E_x (E_x *u + E_y *v + E_t),$$

$$(\alpha^2 + E_x^2 + E_y^2)(v - *v) = -E_y (E_x *u + E_y *v + E_t).$$

2.5 Iterative algorithm

We now have a pair of equations for each point in the image. Using the iterative algorithm proposed by Horn and Schunck [2], we can compute a new set of velocity estimates (u^{n+1}, v^{n+1}) from the estimated derivatives and the average of the previous velocity estimates (u^n, v^n) by

$$u^{n+1} = *u^n - E_x(E_x *u^n + E_y *v^n + E_t) / (\alpha^2 + E_x^2 + E_y^2),$$

$$v^{n+1} = *v^n - E_y(E_x *u^n + E_y *v^n + E_t) / (\alpha^2 + E_x^2 + E_y^2).$$

The natural boundary conditions for the variational problem turns out to be a zero normal derivative. At the edge of the image, some of the points needed to compute the local average of velocity lie outside the image. Here we simply copy velocities from adjacent points further in.

Chapter 3

The Unified Optical Flow Field Approach

Based on the new concept of unified optical flow and a four-frame model, a new approach to motion analysis from a sequence of stereo images is presented. A set of fundamental equations is established to connect these six field quantities which can be solved by an iterative algorithm. Another set of equation is developed for reconstructing 3-D motion field from the six unified optical flow field quantities [3].

3.1 Imaging geometry

An imaging geometry is shown in Fig 3.1. There O - XYZ and O^R - $X^R Y^R Z^R$ are two Cartesian coordinate systems such that O and O^R are the centers of the left and right lenses, respectively. It is assumed in this chapter that the two optical axes OZ and $O^R Z^R$ are on the same plane. The axes OX and $O^R X^R$ are, respectively, perpendicular to OZ and $O^R Z^R$ such that the four axes: OZ , $O^R Z^R$, OX , and $O^R X^R$ are coplanar. The axis OY is not drawn in Figure 3.1 and is understood as being perpendicular to XOZ plane; $O^R Y^R$ is the corresponding component associated with O^R - $X^R Y^R Z^R$. The distance between two lens centers is OO^R denoted by l . The angle between OX and $O^R X^R$ is denoted by ϕ . It is also the angle between the two optical axes: OZ and $O^R Z^R$.

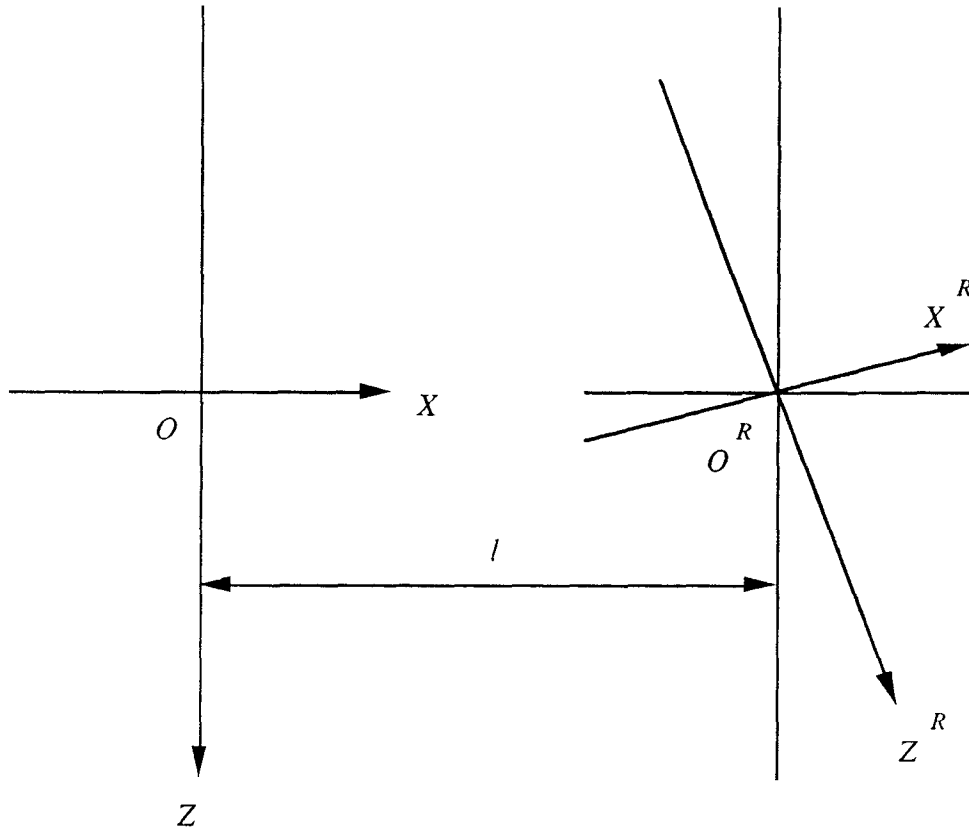


Fig 3.1. Imaging geometry

Consider a world point P in 3-D space. Its coordinates in the two coordinate systems are (X, Y, Z) and (X^R, Y^R, Z^R) , respectively. According to the transformation of coordinate systems in analytic geometry, the relationship between the two coordinates can be expressed as follows.

$$\begin{pmatrix} X^R \\ Y^R \\ Z^R \end{pmatrix} = R \cdot \begin{pmatrix} X \\ Y \\ Z \end{pmatrix} + T \quad (3.1)$$

where R is a rotation matrix

$$R = \begin{pmatrix} \cos\varphi & 0 & -\sin\varphi \\ 0 & 1 & 0 \\ \sin\varphi & 0 & \cos\varphi \end{pmatrix} \quad (3.2)$$

and T is a translation vector.

$$T = \begin{pmatrix} -l \\ 0 \\ 0 \end{pmatrix} \quad (3.3)$$

In Figure 3.2 the focal plane of the left camera is depicted. There $o^L-x^Ly^Lz^L$ is the coordinate system with o^L being the center of the focal plane; o^Lz^L aligned with OZ ; o^Lx^L and o^Ly^L parallel to OX and OY , respectively. The distance Oo^L is the focus length f^L . When a world point is far from cameras, its image can be considered on the focal plane $x^Lo^Ly^L$. It is obvious that a world point P of (X, Y, Z) will have its image point in the $o^L-x^Ly^Lz^L$ coordinate system with coordinate (x^L, y^L, o) . It follows from geometric optics that

$$x^L = \frac{f^L}{Z} X \quad (3.4)$$

$$y^L = \frac{f^L}{Z} Y \quad (3.5)$$

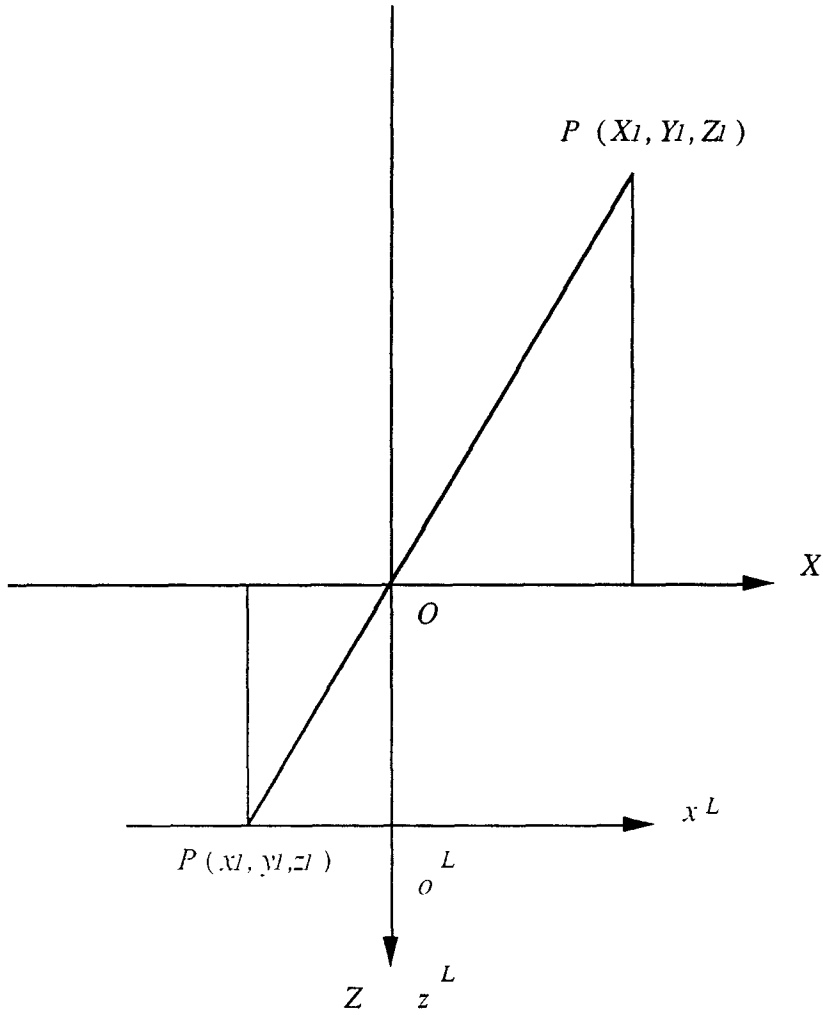


Fig. 3.2. The focal plane of the left camera

For the right camera, the coordinate system $o^R-x^Ry^Rz^R$ can be established similarly.

The following relations are also valid.

$$x^R = \frac{f^R}{Z^R} X^R \quad (3.6)$$

$$y^R = \frac{f^R}{Z^R} Y^R \quad (3.7)$$

For the simplicity, the two cameras are assumed to be identical, thus $f^L = f^R = f$.

Equations (3.4 -- 3.7) become

$$x^L = \frac{f}{Z} X \quad (3.8)$$

$$y^L = \frac{f}{Z} Y \quad (3.9)$$

$$x^R = \frac{f}{Z^R} X^R \quad (3.10)$$

$$y^R = \frac{f}{Z^R} Y^R \quad (3.11)$$

The use of the relation between (X, Y, Z) and (X^R, Y^R, Z^R) derived previously leads to

$$x^R = f \frac{(X-l) \cos \varphi - Z \sin \varphi}{X \sin \varphi + Z \cos \varphi} \quad (3.12)$$

$$y^R = f \frac{Y}{X \sin \varphi + Z \cos \varphi} \quad (3.13)$$

Under the far-field assumption, $Z \approx Z^R$, the above equation can be approximated as

$$x^R = \frac{f}{Z} ((X-l) \cos \varphi - Z \sin \varphi) \quad (3.14)$$

$$y^R = \frac{f}{Z} Y \quad (3.15)$$

3.2 Four-frame model

The four images shown in Figure 3.3 are chosen from a stereo image sequence where images (a) and (c) are taken by the left camera at moments t and $t_I = t + \Delta t$, respectively, images (b) and (d) by the right camera at t and t_I , respectively. Images (a) and (b) are a pair of stereo images at t , images (c) and (d) are a pair of stereo images at t_I . In this chapter the image brightness at the point (x, y) on the image plane at time t is denoted by $g(x, y, t)$ with superscripts indicating which camera is associated with.

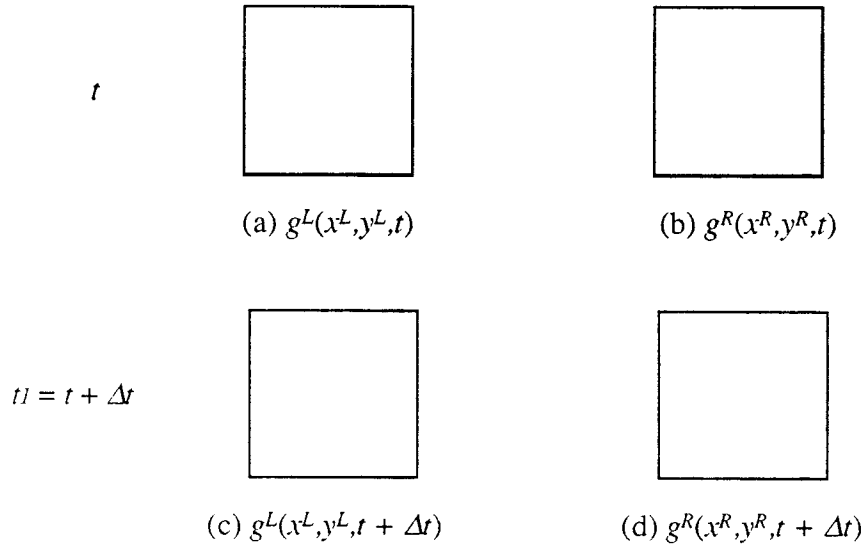


Fig. 3.3. Four frame model

The following derivations are based on these four images chosen from a sequence of stereo images. They are referred to as the four-frame model.

3.3 Unified optical flow field

Following the equations in Chapter 2. and the new concept of unified optical flow field [3,4,5], we define the six field quantities: u^L , v^L , u^R , v^R , u^S , and v^S .

$$u^L = \frac{\Delta \partial x^L}{\partial t} \quad \text{and} \quad v^L = \frac{\Delta \partial y^L}{\partial t};$$

$$u^R = \frac{\Delta \partial x^R}{\partial t} \quad \text{and} \quad v^R = \frac{\Delta \partial y^R}{\partial t};$$

$$u^S = \frac{\Delta \partial x^S}{\partial s} \quad \text{and} \quad v^S = \frac{\Delta \partial y^S}{\partial s}.$$

And we have a set of fundamental equations, and see [3,9] for detail derivation.

$$(g_{xx}^L)^2 u^L + g_{xx}^L g_{yy}^L v^L = \alpha^2 \nabla^2 u^L - g_{xx}^L g_{tt}^L,$$

$$g_{xx}^L g_{yy}^L u^L + (g_{xx}^L)^2 v^L = \alpha^2 \nabla^2 v^L - g_{xx}^L g_{tt}^L,$$

$$(g_{xx}^R)^2 u^R + g_{xx}^R g_{yy}^R v^R = \alpha^2 \nabla^2 u^R - g_{xx}^R g_{tt}^R,$$

$$g_{xx}^R g_{yy}^R u^R + (g_{xx}^R)^2 v^R = \alpha^2 \nabla^2 v^R - g_{xx}^R g_{tt}^R,$$

$$(g_{xx}^S)^2 u^S + g_{xx}^S g_{yy}^S v^S = \alpha^2 \nabla^2 u^S - g_{xx}^S g_{ss}^S,$$

$$g_{xx}^S g_{yy}^S u^S + (g_{xx}^S)^2 v^S = \alpha^2 \nabla^2 v^S - g_{xx}^S g_{ss}^S$$

Since the format of these pairs of equations are the same as ones in Chapter 2. The iterative algorithms introduced in Chapter 2 can be employed here to determine u^R , v^R , u^L , v^L , u^S , and v^S . It can be shown in the next sub-section that these six field quantities contain sufficient information to recover the motion in 3-D space.

3.4 A set of equations for analysis of 3-D motion field

In order to reconstruct 3-D motion field we need to determine the following six quantities: 1) The position of the moving objects: X, Y, Z , and 2) the velocities of the moving objects at the given position: $*X, *Y, *Z$. From the preceding section, we already have u^R, v^R, u^L, v^L, u^S , and v^S . Now following the derivation in [3], we get the relation between these two sets of quantities in this section.

It is obvious that

$$\frac{1}{f} u^R = \frac{1}{f} \frac{\partial X^R}{\partial t}$$

From Equation (3.14), we have

$$\begin{aligned} \frac{1}{f} u^R &= \frac{(*X \cos \varphi - *Z \sin \varphi)Z - [(X - l) \cos \varphi - Z \sin \varphi]*Z}{Z^2} \\ &= \frac{1}{Z^2} [(*XZ - X*Z) \cos \varphi + l*Z \cos \varphi] \\ &= \frac{(*XZ - X*Z) \cos \varphi}{Z^2} + \frac{l*Z \cos \varphi}{Z^2} \end{aligned}$$

The use of Equation (3.8) leads to

$$\frac{l}{f} u^R (x^R, y^R, t) = \frac{l}{f} u^L (x^L, y, t) + \frac{l * Z}{Z^2} \cos \varphi$$

It follows from Equation (3.15) that

$$\frac{l}{f} v^R (x^R, y^R, t) = \frac{l}{f} v^L (x, y, t)$$

The following equations relating the spatial variation rates, u^S and v^S , to the imaging setting parameters, l, φ, f , the characteristic length, χ , and 3-D space coordinate, X, Y , and Z are derived in Appendix A of [3].

$$\frac{u^S}{f} = - \left(\frac{l \cos \varphi}{Z} + \frac{2 (l - \cos \varphi)}{\sin \varphi} \right) / \sqrt{l^2 + \chi^2 \varphi^2}$$

$$\frac{v^S}{f} = 0$$

Again the approximation, replacing derivative by average variation rate, is made in deriving the following two equations.

$$u^S = \frac{x^R - x^L}{\sqrt{l^2 + \chi^2 \varphi^2}}$$

$$v^S = \frac{y^R - y^L}{\sqrt{l^2 + \chi^2 \varphi^2}}$$

Finally, we have a set of equations used for reconstructing:

$$Z = - \frac{f l \sin \varphi \cos \varphi}{u^S \sqrt{l^2 + \chi^2 \varphi^2} \sin \varphi + 2 f (1 - \cos \varphi)} \quad (3.16)$$

$$X = \frac{x^L Z}{f} \quad (3.17)$$

$$Y = \frac{y^L Z}{f} \quad (3.18)$$

$$x^R = u^S \sqrt{l^2 + \chi^2 \varphi^2} + x^L \quad (3.19)$$

$$y^R = u^S \sqrt{l^2 + \chi^2 \varphi^2} + y^L \quad (3.20)$$

$${}^*Z = \frac{(u^R - u^L \cos \varphi) Z^2}{l f \cos \varphi} \quad (3.21)$$

$${}^*X = \frac{u^L Z}{f} + \frac{{}^*Z X}{Z} \quad (3.22)$$

$${}^*Y = \frac{v^L Z}{f} + \frac{{}^*Z Y}{Z} \quad (3.23)$$

It can be seen that in Equations (3.16-23) all quantities on the right-hand sides are either the imaging setting parameters or the unified optical flow field quantities. That is, they are available. Quantities x^R and y^R on the left-hand sides of Equations (3.19-20), respectively, are used to determine which value of u^R should be utilized in Equation (3.21) to calculate *Z . All quantities on the left-hand sides of Equations (3.16-18, 3.21-23), being the motion parameters: position and velocity in 3-D space, are therefore can be solved straightforward.

Chapter 4

A Simulation Process

The algorithms introduced in Chapters 2 and 3 are implemented in this thesis work. And it is demonstrated that the UOFF approach is feasible and efficient .

4.1 Setting

In this thesis, a rotatable sphere with the radius of R is the object in experiments. Fig. 4.1 shows the simulation setting.

The center of sphere is O' , and the $O'-X'Y'Z'$ of the sphere is a 3-D Cartesian coordinate system. There are two sensors in this imaging setting. There $O^L-X^LY^LZ^L$ and $O^R-X^RY^RZ^R$ are two Cartesian coordinate systems such that O^L and O^R are the centers of the left and right lenses, respectively. The relation between $O'-X'Y'Z'$ and $O^L-X^LY^LZ^L$ is as follows. The axes $O'Z'$ and O^LZ^L are aligned. The axes $O'X'$ and O^LX^L are parallel, and $O'Y'$ and O^LY^L are parallel. For the sake of simplicity, the axes O^RX^R , O^RY^R , and O^RZ^R are not drawn in Fig. 4.1. The relation between $O^L-X^LY^LZ^L$ and $O^R-X^RY^RZ^R$ is described next. The axes O^RZ^R and O^RX^R are on the $X^LO^LZ^L$ plane, The axes O^LY^L and O^RY^R are parallel. The two sensors are assumed to be identical with focal length f . The angle between the optical axes of the two sensors is denoted by φ , and the distance between the two sensors is l

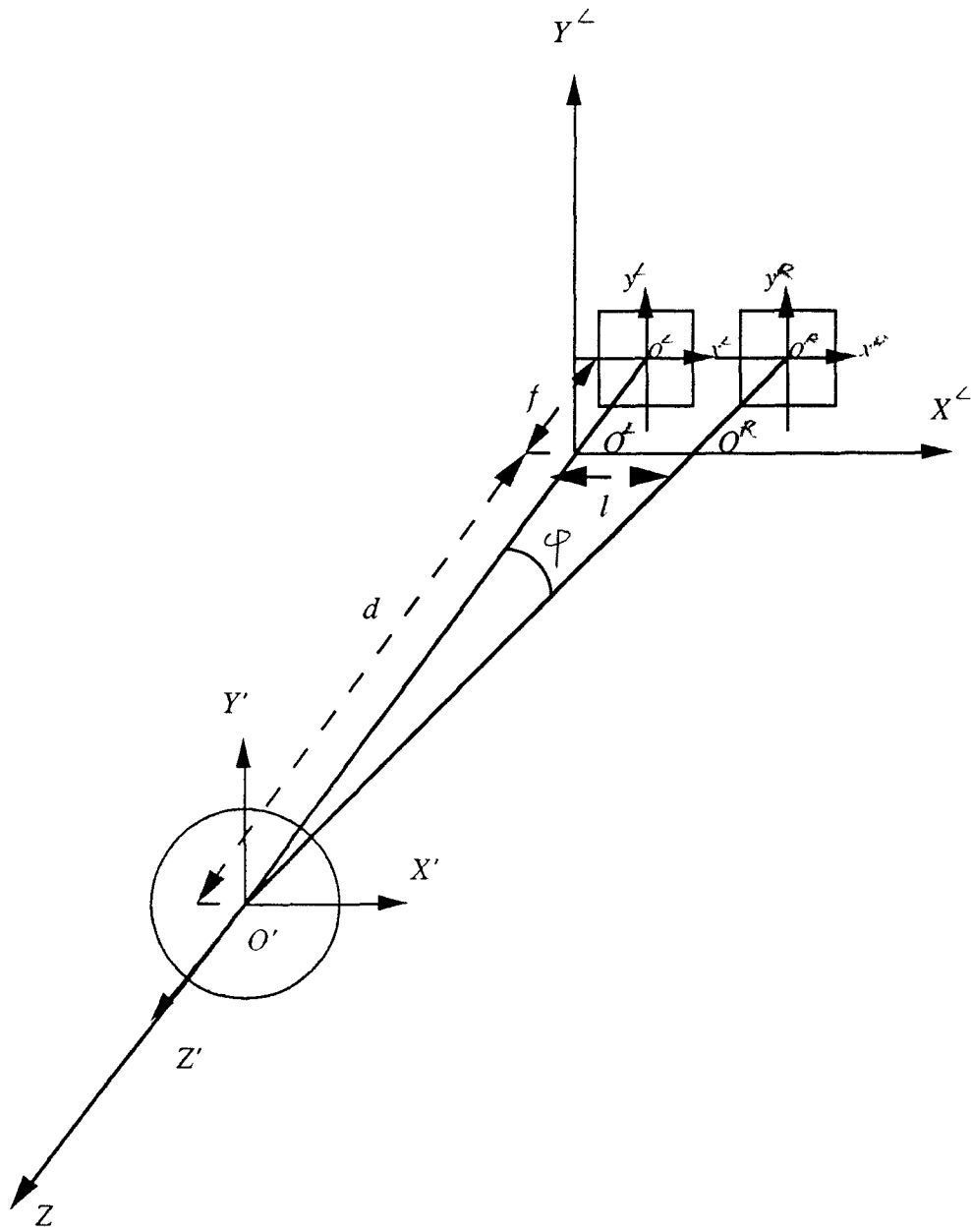


Fig. 4.1 Setting

The distance between the O' of the sphere and the center of the left sensor is denoted by d , and the counterpart for the right sensor is $d/\cos\varphi$.

The 2-D Cartesian coordinate systems for the image planes are $o^L-x^Ly^L$ and $o^R-x^Ry^R$.

The sphere which is redrawn in Fig.4.2 is rotatable. $P (X',Y',Z')$ denotes an arbitrary point on the sphere surface. The angle between the axis $O'Y'$ and $O'P$ is denoted by ϕ_I , and the angle between the $O'Z'$ and the projection of $O'P$ on $X'O'Z'$ plane, $O'P'$, is denoted by θ_I .

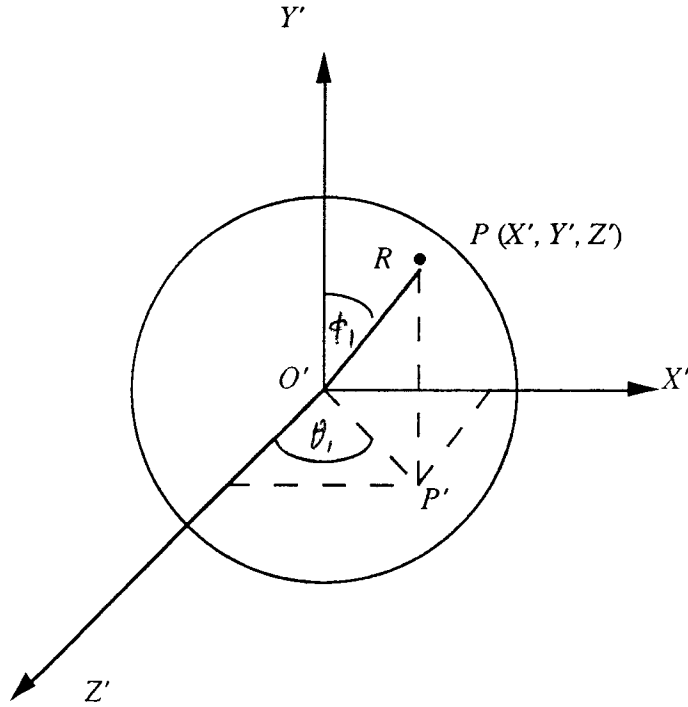


Fig. 4.2. The rotatable sphere

It is assumed that the basic brightness function of the sphere's surface is a sinusoidal function:

$$g = \text{Int} [127.5 \sin (\theta_I) \sin (\phi_I) + 127.5] \quad (4.1)$$

where Int denotes taking integrate part of the argument, θ_I and ϕ_I are defined as

$$\theta_I = \arctan (X'/Z')$$

$$\phi_I = \arccos (Y'/R),$$

In Fig. 4.3, it is obvious that a world point P of (X', Y', Z') will have its image point in the xoy image plane. The axes $O'X'$, OX , and ox are not drawn in Fig.4.4 and they are understood as being perpendicular to $Y'O'Z'$, YOZ , and yoz planes, respectively. It follows from geometric optics that

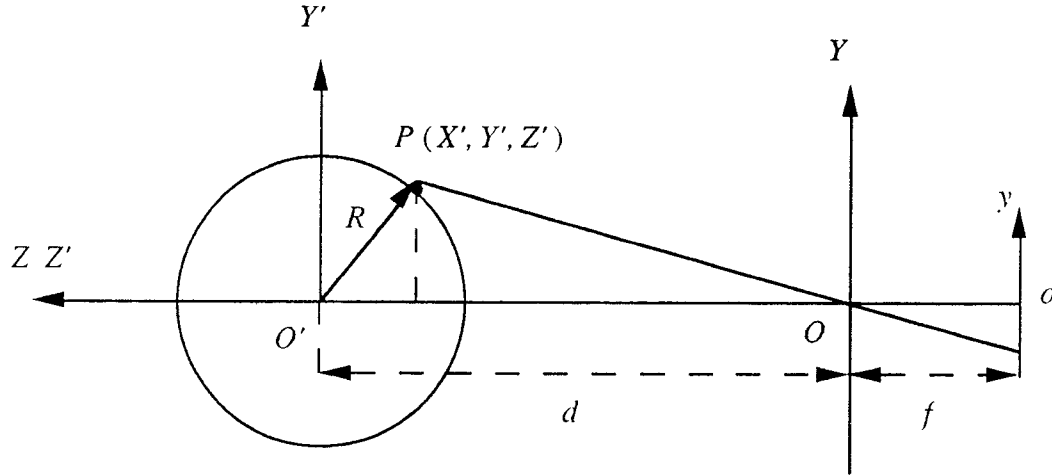


Fig. 4.3. Perspective projection

$$\frac{x}{f} = \frac{-X'}{d + Z'} \quad (4.2)$$

$$\frac{y}{f} = \frac{-Y'}{d + Z'} \quad (4.3)$$

And we know the equation for the sphere is:

$$X'^2 + Y'^2 + Z'^2 = R^2 \quad (4.4)$$

Combining the above three equations (4.2 - 4.4), we can solve for Z' .

$$Z' = \frac{-d(x^2 + y^2) - \sqrt{d^2(x^2 + y^2)^2 - (f^2 + x^2 + y^2)[d^2(x^2 + y^2) - f^2R^2]}}{f^2 + x^2 + y^2} \quad (4.5)$$

in which we restrict

$$d^2 (x^2 + y^2)^2 \geq (f^2 + x^2 + y^2) [d^2 (x^2 + y^2) - f^2 R^2]$$

Once Z' is solved, X' and Y' can be easily obtained as follows,

$$X' = \frac{-x(d + Z')}{f} \quad (4.6)$$

$$Y' = \frac{-y(d + Z')}{f} \quad (4.7)$$

The next three equations follow from Fig.4.2 easily.

$$X' = R \sin \phi_I \sin \theta_I \quad (4.8)$$

$$Y' = R \cos \phi_I \quad (4.9)$$

$$Z' = R \sin \phi_I \cos \theta_I \quad (4.10)$$

4.2 Simulation

Assume the sphere is only experiencing rotation around Y' axis. There is no translation, and no rotation around X' and Z' axes

There are three steps in our simulation process,

Step 1: Generate simulation image data: Images a), b), c), and d), as shown in Fig.4.4.

During the time interval $t_2 - t_1$, the angle rotated by the sphere around the axis Y' is denoted by θ_2 , and the angle rotated around the axis X' is denoted by ϕ_2 . It is noted that the directions of the rotations are, respectively, anticlockwise when looking from Y' to O' and

from X' to O' . In the simulation conducted in this thesis work, only θ_2 is considered, i.e., it is assumed that $\phi_2=0$.

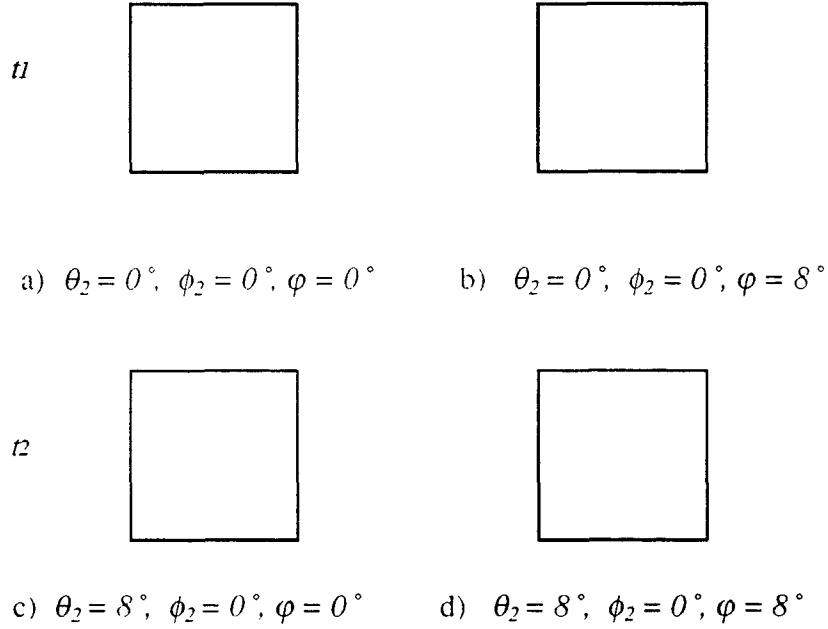


Fig. 4.4. The four images

For Image a): We know that for any pair of x and y on the picture plane we can find the coordinates of the corresponding point in 3-D space, i.e., X' , Y' , and Z' by using Eqs.(4.5-7). The use of Eqs.(4.8-10) will then lead to finding out θ_l and ϕ_l .

At the first moment t_l for the left sensor, the brightness function is determined as follows.

$$g_a = \text{Int} [127.5 \sin (\theta_l) \sin (\phi_l) + 127.5]$$

where

$$\theta_l = \arctan (X'/Z')$$

$$\phi_l = \arccos (Y'/R)$$

the notation Int means taking the integer part of the respective argument.

For Image c): At the second moment t_2 , the sphere is rotated by θ_2 . For the same left sensor, the brightness function is defined as

$$g_c = \text{Int} [127.5 \sin (\theta_l - \theta_2) \sin (\phi_l) + 127.5]$$

For Image b): At the first moment t_1 consider the right sensor, since the angle between the sensors is φ . the brightness function can be determined according to

$$g_b = \text{Int} [127.5 \sin (\theta_l - \varphi) \sin (\phi_l) + 127.5]$$

For Image d): At the second moment t_2 for the right sensor, the brightness function is related to

$$g_d = \text{Int} [127.5 \sin (\theta_l - \varphi - \theta_2) \sin (\phi_l) + 127.5]$$

Step 2: Determine the UOFF quantities, u^L , v^L , u^R , v^R , u^S , and v^S . In Chapter 2, the following two equations have been obtained, by which u and v can be determined.

$$u^{n+1} = *u^n - E_x (E_x *u^n + E_y *v^n + E_t) / (\alpha^2 + E_x^2 + E_y^2),$$

$$v^{n+1} = *v^n - E_y (E_x *u^n + E_y *v^n + E_t) / (\alpha^2 + E_x^2 + E_y^2).$$

A program has been written to determine u and v according to the above iterative equations. The inputs and the outputs of the program are listed below:

<u>INPUT</u>	<u>OUTPUT</u>
Image a) and Image c)	u^L and v^L
Image b) and Image d)	u^R and v^R
Image a) and Image b)	u^S and v^S

In this simulation step, there are two variables which need to be chosen: α and n .

The α is a suitable weighting factor. If we use a large value of α , the solution will be very stable, but too smooth; if we use a small value of α , the solution will be more noisy, but more faithful to the actual flow [2].

In our experiments, we tried to start the α at a high value (100) and gradually decreased it until things become unstable (0). We found that when the α is among from 10 to 0.1, the results is of stable, and finally we choose the $\alpha = 10$ in our experiments.

The n is the numbers of the iterations, and because lots of CPU time will be taken away by iterating the algorithms, we have to limit the n to a reasonable value.

For instance, when the image matrix is of 128×128 , it would need at least 128 iterations. And if we want to get a better simulating result, the numbers of iteration will be several times of the image' size (128)

By the testing, we fount out that if $n = 2 \times \text{image size}$, the result is improved obviously. So in our experiments, we choose $n = 2 \times \text{size}$.

Step 3: Reconstruct the 3-D position X, Y, Z and motion $*X, *Y, *Z$. We use the equations introduced in Chapter 3 to recover the position and motion of the sphere. And the equations are relisted below.

$$Z = - \frac{f l \sin \varphi \cos \varphi}{u^S \sqrt{l^2 + \chi^2 \varphi^2} \sin \varphi + 2 f (1 - \cos \varphi)}$$

$$X = \frac{x^L Z}{f}$$

$$Y = \frac{y^L Z}{f}$$

$$x^R = u^S \sqrt{l^2 + \chi^2 \varphi^2} + x^L$$

$$y^R = u^S \sqrt{l^2 + \chi^2 \varphi^2} + y^L$$

$$*Z = \frac{(u^R - u^L \cos \varphi) Z^2}{l f \cos \varphi}$$

$$*X = \frac{u^L Z}{f} + \frac{*Z X}{Z}$$

$$*Y = \frac{y^L Z}{f} + \frac{*Z Y}{Z}$$

4.3 Analytic solution

In order to estimate the results of simulation, we must know the accurate values of u^L , v^L , u^R , v^R , u^S , and v^S for each pixel in the picture, and the accurate values of Z , X , Y , $*Z$, $*X$, and $*Y$ for each points on the sphere surface that has been perspectively projected to the images. Since the simulation images are set up by ourselves, we could figure out everything that we need.

Estimation of u^L and v^L :

At the first moment t_1 , we have a pair of $x_{t_1}^L$ and $y_{t_1}^L$ on the picture plane, and using Eqs.(4.5-7) we can get the coordinates of the corresponding point in 3-D space, i.e., $X_{t_1}^L$, $Y_{t_1}^L$, and $Z_{t_1}^L$

And at the second moment t_2 , the sphere is rotated by $\Delta\theta_2$. We can use Eqs.(4.8-10) to get $X_{t_2}^L$, $Y_{t_2}^L$, and $Z_{t_2}^L$ on the sphere surfac. That is,

$$X_{t_2}^L = R \sin \phi_{1,t_1} \sin (\theta_{1,t_1} + \Delta\theta_2)$$

$$Y_{t_2}^L = R \cos \phi_{1,t_1}$$

$$Z_{t_2}^L = R \sin \phi_{1,t_1} \cos (\theta_{1,t_1} + \Delta\theta_2)$$

where

$$\theta_{1,t_1} = \arctan (X_{t_1}^L / Z_{t_1}^L)$$

$$\phi_{1,t_1} = \arccos (Y_{t_1}^L / R)$$

Using Eqs.(4.2-3), we can get $x_{t_2}^L$ and $y_{t_2}^L$ as follows

$$x_{t_2}^L = \frac{-X_{t_2}^L f}{d + Z_{t_2}^L}$$

$$y_{t2}^L = \frac{-Y_{t2}^L f}{d + Z_{t2}^L}$$

Finally we have:

$$u^L = (x_{t2}^L - x_{t1}^L)/(t2 - t1)$$

$$v^L = (y_{t2}^L - y_{t1}^L)/(t2 - t1)$$

Estimation of u^R and v^R :

According to the rotation transformations Eqs.(3.1-3), and the fact that the angle between the optical axes of the two sensors is φ , we can get X'^R_{t1} , Y'^R_{t1} , Z'^R_{t1} , X'^R_{t2} , Y'^R_{t2} , and Z'^R_{t2} from X'^L_{t1} , Y'^L_{t1} , Z'^L_{t1} , X'^L_{t2} , Y'^L_{t2} , and Z'^L_{t2} .

$$X'^R_{t1} = -Z'^L_{t1} \sin \varphi + X'^L_{t1} \cos \varphi$$

$$Y'^R_{t1} = Y'^L_{t1}$$

$$Z'^R_{t1} = Z'^L_{t1} \cos \varphi + X'^L_{t1} \sin \varphi$$

$$X'^R_{t2} = -Z'^L_{t2} \sin \varphi + X'^L_{t2} \cos \varphi$$

$$Y'^R_{t2} = Y'^L_{t2}$$

$$Z'^R_{t2} = Z'^L_{t2} \cos \varphi + X'^L_{t2} \sin \varphi$$

Using Eqs.(4.2-3), we have,

$$x'^R_{t1} = \frac{-X'^R_{t1} f}{d / \cos \varphi + Z'^R_{t1}}$$

$$y'^R_{t1} = \frac{-Y'^R_{t1} f}{d / \cos \varphi + Z'^R_{t1}}$$

$$x^R_{t2} = \frac{-X^R_{t2}f}{d / \cos \varphi + Z^R_{t2}}$$

$$y^R_{t2} = \frac{-Y^R_{t2}f}{d / \cos \varphi + Z^R_{t2}}$$

Therefore

$$u^R = (x^R_{t2} - x^R_{t1}) / (t2 - t1)$$

$$v^R = (y^R_{t2} - y^R_{t1}) / (t2 - t1)$$

Estimation of u^S and v^S :

To a pair of x^L_{t1} and y^L_{t1} associated with the left sensor, we have X^L_{t1} , Y^L_{t1} , and Z^L_{t1} representing a point on the sphere surface

For the right sensor we know that the angle between the sensors is φ , and use Eqs.(4.8-10) we have:

$$X^R_{t1} = R \sin \phi_{1,t1} \sin (\theta_{1,t1} - \varphi)$$

$$Y^R_{t1} = R \cos \phi_{1,t1}$$

$$Z^R_{t1} = R \sin \phi_{1,t1} \cos (\theta_{1,t1} - \varphi)$$

where

$$\theta_{1,t1} = \arctan (X^L_{t1} / Z^L_{t1})$$

$$\phi_{1,t1} = \arccos (Y^L_{t1} / R)$$

So using Eq.(4.2-3), we could get:

$$x^R_{t1} = \frac{-X^R_{t1}f}{d + Z^R_{t1}}$$

$$y^R_{tl} = \frac{-Y^R_{tl} f}{d + Z^R_{tl}}$$

Finally we have

$$u^S = (x^R_{tl} - x^L_{tl}) / \Delta s$$

$$v^S = (y^R_{tl} - y^L_{tl}) / \Delta s$$

Estimation of Z , X , Y , $*Z$, $*X$, and $*Y$:

At the first moment t_1 , suppose that a point on the picture plane is (x^L_{t1}, y^L_{t1}) . Using Eqs.(4.5-7) we can find out the x^L_{t1} , y^L_{t1} , and z^L_{t1} . The X , Y , and Z are therefore can be recovered as

$$X = x^L_{t1},$$

$$Y = y^L_{t1},$$

$$Z = z^L_{t1} + d.$$

From Eqs (4 8-10), the sphere can be described as

$$X' = R \sin \phi_1 \sin \theta_1$$

$$Y' = R \cos \phi_1$$

$$Z' = R \sin \phi_1 \cos \theta_1$$

The velocities of $*X$, $*Y$, and $*Z$ can be obtained from the following equations,

$$*X = \frac{dX}{dt} = \frac{\partial X}{\partial \theta_1} \frac{\partial \theta_1}{\partial t} + \frac{\partial X}{\partial \phi_1} \frac{\partial \phi_1}{\partial t} = R \sin \phi_1 \cos \theta_1 \frac{\partial \theta_1}{\partial t}$$

$$*Y = \frac{dY}{dt} = \frac{dY}{d\phi_1} \frac{d\phi_1}{dt} = 0$$

$$*Z = \frac{dZ}{dt} = \frac{\partial Z}{\partial \theta_1} \frac{\partial \theta_1}{\partial t} + \frac{\partial Z}{\partial \phi_1} \frac{\partial \phi_1}{\partial t} = -R \sin \phi_1 \sin \theta_1 \frac{\partial \theta_1}{\partial t}$$

where

$$\frac{\partial \theta_1}{\partial t} = \frac{\Delta \theta_1}{\Delta t} = \Delta \theta_2 \quad (\text{ assume } \Delta t = 1)$$

$$\frac{\partial \phi_1}{\partial t} = \frac{\Delta \phi_1}{\Delta t} = \Delta \phi_2 = 0 \quad (\text{ in our experiments })$$

4.4 Comparison

In the whole experiments, the related parameters are:

The image size. 32×32 (or 128×128)

The focus distance: l

The objective distance: 140

The radius of the sphere: 10

The angle rotated around axis Y' : 8.0°

The angle rotated around axis X' : 0.0°

The angle between the two sensors: 8.0°

The α : 10

The number of iteration: 64 (or 256)

We are only given the four images for the analysis of the motion. Using the new methods developed in Chapters 2 and 3, we can determine a set of values (u^L , v^L , u^R , v^R , u^S , and v^S) on the picture planes, and further derive another set of values (X , Y , Z , $*X$, $*Y$, $*Z$) for the object in 3-D space.

And we can also use the mathematical formulae discussed in Section 3 to figure out what the exact values are.

The errors between the simulation values and exact values are estimated in our experiments according to

$$\text{error \%} = \frac{\text{Analytic value} - \text{Simulated value}}{\text{Analytic value}} \times 100$$

Figs. 4.5, 4.6 and 4.7 show the final results.

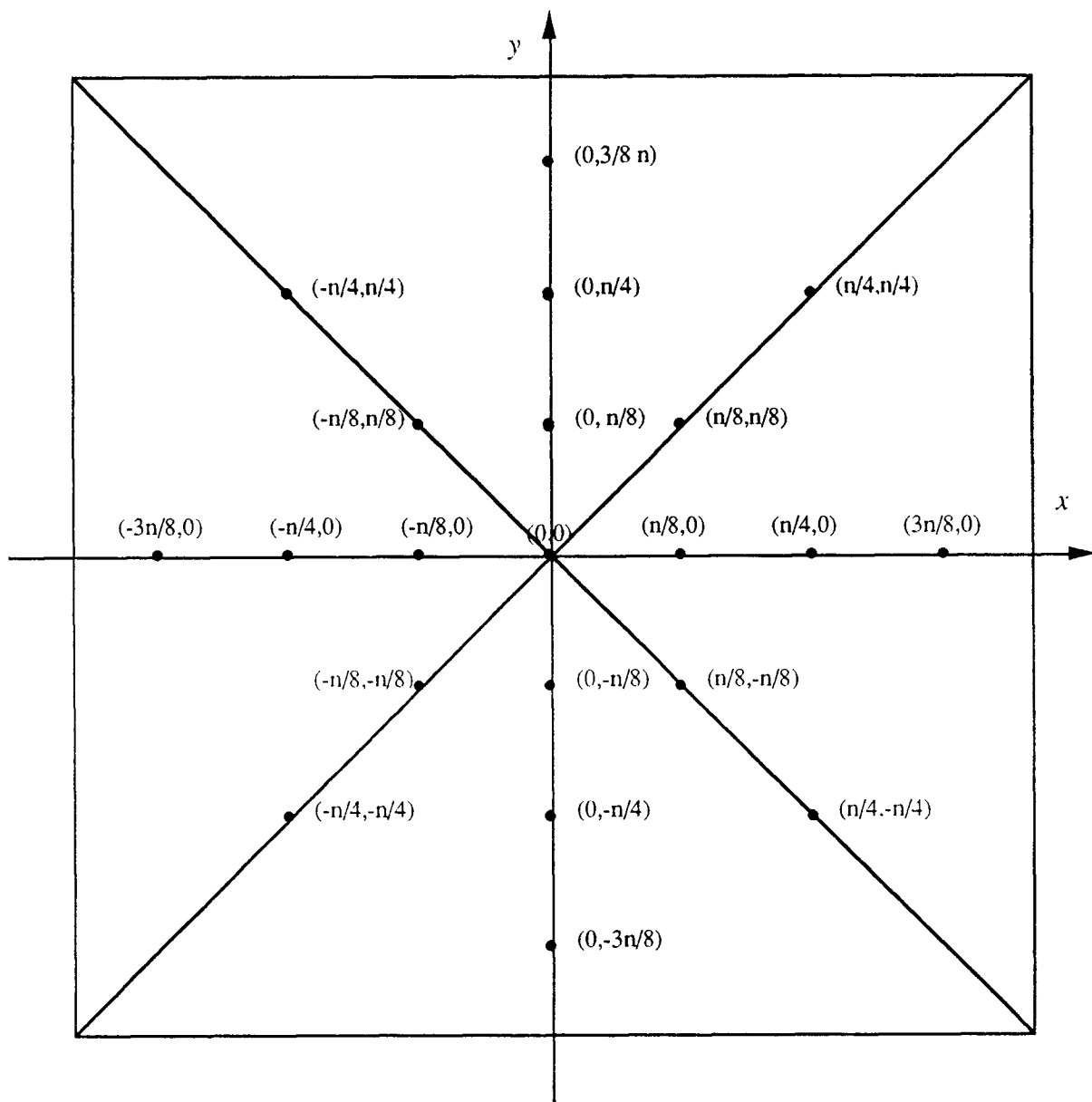


Fig. 4.5. The sample pixels

x, y	X			Y			Z		
	Analytic	Simulate	Error	Analytic	Simulate	Error	Analytic	Simulate	Error
12, 0	-8.22303	-8.27642	-0.65	0.00000	0.00000	0.00	-134.30950	-135.18161	-0.65
8, 0	-5.36996	-5.37448	-0.08	0.00000	0.00000	0.00	-131.56414	-131.67492	-0.08
4, 0	-2.66041	-2.65946	0.04	0.00000	0.00000	0.00	-130.36038	-130.31372	0.04
0, 0	0.00000	0.00000	0.00	0.00000	0.00000	0.00	-130.00000	-130.13107	-0.10
-4, 0	2.66041	2.65612	0.16	0.00000	0.00000	0.00	-130.36038	-130.15007	0.16
-8, 0	5.36996	5.35715	0.24	0.00000	0.00000	0.00	-131.56414	-131.25027	0.24
-12, 0	8.22303	8.21093	0.15	0.00000	0.00000	0.00	-134.30950	-134.11184	0.15
0, 12	0.00000	0.00000	0.00	-8.22303	-8.26821	-0.55	-134.30950	-134.04750	-0.55
0, 8	0.00000	0.00000	0.00	-5.36996	-5.38608	-0.30	-131.56414	-131.95916	-0.30
0, 4	0.00000	0.00000	0.00	-2.66041	-2.67037	-0.37	-130.36038	-130.84820	-0.37
0, -4	0.00000	0.00000	0.00	2.66041	2.67518	-0.56	-130.36038	-131.08406	-0.56
0, -8	0.00000	0.00000	0.00	5.36996	5.40811	-0.71	-131.56414	-132.49876	-0.71
0, -12	0.00000	0.00000	0.00	8.22303	8.36564	-1.73	-134.30950	-136.63890	-1.73
8, 8	-5.45454	-5.47716	-0.41	-5.45454	-5.47716	-0.41	-133.63636	-134.19058	-0.41
4, 4	-2.66814	-2.66625	0.07	-2.66814	-2.66625	0.07	-130.73922	-130.64663	0.07
-4, -4	2.66814	2.67404	-0.22	2.66814	2.67404	-0.22	-130.73922	-131.02807	-0.22
-8, -8	5.45454	5.46612	-0.21	5.45454	5.46612	-0.21	-133.63636	-133.92015	-0.21
-8, 8	5.45454	5.44605	0.16	-5.45454	-5.44605	0.16	-133.63636	-133.42826	0.16
-4, 4	2.66814	2.66953	-0.05	-2.66814	-2.66953	-0.05	-130.73922	-130.80699	-0.05
4, -4	-2.66814	-2.67860	-0.39	2.66814	2.67860	-0.39	-130.73922	-131.25163	-0.39
8, -8	-5.45454	-5.48905	-0.63	5.45454	5.48905	-0.63	-133.63636	-134.48175	-0.63
			%			%			%

Fig. 4.6 (a) The table of results (n = 32).

x, y	*X			*Z		
	Analytic	Simulate	Error	Analytic	Simulate	Error
12, 0	-0.79454	-0.75748	4.66	1.14815	1.48394	-29.17
8, 0	-1.17786	-1.14682	2.64	0.74978	1.09195	-45.64
4, 0	-1.34594	-1.36573	-1.47	0.37146	0.72063	-94.00
0, 0	-1.39626	-1.42866	-2.34	0.00000	0.30662	-----
-4, 0	-1.34594	-1.36611	-1.50	-0.37146	-0.14864	59.99
-8, 0	-1.17786	-1.20914	-2.66	-0.74978	-0.86843	-15.82
-12, 0	-0.79794	-0.87709	-10.39	-1.14815	-0.89299	22.22
0, 12	-0.79454	-0.74128	6.70	0.00000	0.00382	-----
0, 8	-1.17786	-1.17106	0.58	0.00000	0.09913	-----
0, 4	-1.34594	-1.31396	2.38	0.00000	0.07285	-----
0, -4	-1.34594	-1.35563	-0.72	0.00000	0.54498	-----
0, -8	-1.17786	-1.13661	3.50	0.00000	0.25060	-----
0, -12	-0.79454	-0.54849	30.97	0.00000	0.02952	-----
8, 8	-0.88853	-0.89746	-1.01	0.76159	1.09657	-43.98
4, 4	-1.29304	-1.28022	0.99	0.37254	0.40286	-8.14
-4, -4	-1.29304	-1.24656	3.59	-0.37254	0.54037	-45.05
-8, -8	-0.88853	-0.84169	5.27	-0.76159	-0.82264	-8.02
-8, 8	-0.88853	-0.95307	-7.26	-0.76159	-0.37234	51.11
-4, 4	-1.29304	-1.28404	0.70	-0.37254	-0.41045	-10.18
4, -4	-1.29304	-1.23005	4.87	0.37254	0.37383	-0.35
8, -8	-0.88853	-0.71180	19.89	0.76159	0.52983	30.43
			%			%

Fig. 4.6.(b) The table of results (n = 32).

	X			Y			Z		
x, y	Analytic	Simulate	Error	Analytic	Simulate	Error	Analytic	Simulate	Error
48,0	-8.22303	-8.21015	0.16	0.00000	0.00000	0.00	134.30950	134.09910	0.16
32,0	-5.36996	-5.34872	0.40	0.00000	0.00000	0.00	131.56414	131.04393	0.40
16,0	-2.66041	-2.64719	0.50	0.00000	0.00000	0.00	130.36038	129.71275	0.50
0,0	0.00000	0.00000	0.00	0.00000	0.00000	0.00	130.00000	129.34632	0.50
-16,0	2.66041	2.64655	0.52	0.00000	0.00000	0.00	130.36038	129.68096	0.52
-32,0	5.36996	5.34422	0.48	0.00000	0.00000	0.00	131.56414	130.93342	0.48
-48,0	8.22303	8.19257	0.37	0.00000	0.00000	0.00	134.30950	133.81202	0.37
0,48	0.00000	0.00000	0.00	-8.22303	-8.22616	-0.04	134.30950	134.36073	-0.04
0,32	0.00000	0.00000	0.00	-5.36996	-5.34928	0.39	131.56414	131.05757	0.39
0,16	0.00000	0.00000	0.00	-2.66041	-2.64671	0.52	130.36038	129.68899	0.52
0,-16	0.00000	0.00000	0.00	2.66041	2.65250	0.30	130.36038	129.97291	0.30
0,-32	0.00000	0.00000	0.00	5.36996	5.36499	0.09	131.56414	131.44229	0.09
0,-48	0.00000	0.00000	0.00	8.22303	8.24334	-0.25	134.30950	134.64137	-0.25
32,32	-5.45454	-5.44853	0.11	-5.45454	-5.44853	0.11	133.63636	133.48901	0.11
16,16	-2.66814	-2.65659	0.43	-2.66814	-2.65659	0.43	130.73922	130.17132	0.43
-16,-16	2.66814	2.65732	0.41	2.66814	2.65732	0.41	130.73922	130.20866	0.41
-32,-32	5.45454	5.44559	0.16	5.45454	5.44559	0.16	133.63636	133.41696	0.16
-32,32	5.45454	5.44005	0.27	-5.45454	-5.44005	0.27	133.63636	133.28129	0.27
-16,16	2.66814	2.65614	0.45	-2.66814	-2.65614	0.45	130.73922	130.15101	0.45
16,-16	-2.66814	-2.65941	0.33	2.66814	2.65941	0.33	130.73922	130.31114	0.33
32,-32	-5.45454	-5.45004	0.08	5.45454	5.45004	0.08	133.63636	133.52618	0.08
			%			%			%

Fig. 4.7.(a) The table of results (n = 128).

x, y	*X			*Z		
	Analytic	Simulate	Error	Analytic	Simulate	Error
48,0	-0.79454	0.79454	-2.74	1.14815	1.14815	-15.30
32,0	-1.17786	1.17786	-1.66	0.74978	0.92874	-23.87
16,0	-1.34594	1.34594	-0.60	0.37146	0.48970	-31.83
0,0	-1.39626	1.39626	-0.63	0.00000	0.30297	-----
-16,0	-1.34594	1.34594	-0.37	-0.37146	0.18761	49.49
-32,0	-1.17786	1.17786	-2.12	-0.74978	0.72077	3.87
-48,0	-0.79794	0.85113	-7.12	-1.14815	1.23731	-7.77
0,48	-0.79454	0.79454	12.96	0.00000	0.01911	-----
0,32	-1.17786	1.17786	4.70	0.00000	0.09103	-----
0,16	-1.34594	1.33293	0.97	0.00000	0.19012	-----
0,-16	-1.34594	1.34594	-0.32	0.00000	0.20061	-----
0,-32	-1.17786	1.12203	4.74	0.00000	0.00170	-----
0,-48	-0.79454	0.79454	17.76	0.00000	0.06226	-----
32,32	-0.88853	0.85600	3.66	0.76159	0.95120	-24.90
16,16	-1.29304	1.29304	0.26	0.37254	0.48874	-31.19
-16,-16	-1.29304	1.18150	0.89	-0.37254	0.32376	0.89
-32,-32	-0.88853	0.85231	4.08	-0.76159	0.83620	-9.80
-32,32	-0.88853	0.87957	1.01	-0.76159	0.78034	-2.46
-16,16	-1.29304	1.29304	-0.01	-0.37254	0.24990	32.92
16,-16	-1.29304	1.28507	0.62	0.37254	0.61947	-66.28
32,-32	-0.88853	0.83390	6.15	0.76159	0.92248	-21.12
			%			%

Fig. 4.7.(b) The table of results (n = 128).

Chapter 5

Conclusion and Discussion

1. Recently, based on a four-frame model, the optical flow method is extended from the temporal sequence of images to the spatial sequence of images to establish unified optical flow field characterized by six field quantities. A set of fundamental equations is established to connect these six field quantities which can be solved by an iterative algorithm. Another set of equation is developed for reconstructing 3-D motion field from the six unified optical flow field quantities [3].
2. The reasonably good simulation results have verified the excellent capability of the now approaches.
3. The most difficult problem in motion estimation is feature correspondence. In stereo imagery, the problem is even harder because not only the correspondence in temporal sequences of images but also the correspondence in the pair of stereo images are required. Different from all existing techniques dealing with stereo imagery, this new approach does not require feature correspondence at all because point correspondence is merely an intermediate step in derivation of this new approach. Therefore, it is expected to be much more efficient [3].
4. In this stereo imagery two sensors are usually required to be exactly. In order to eliminate this strict requirement, an upgrade imaging system is developed in [10].

5. The application of the approaches in this thesis is under investigation.

Bibliography

[1] J. K. Aggarwal and N. Nandhakumar, "On the computation of motion from sequences of images - a review," *Proceedings of the IEEE*, vol. 76, no. 8, pp. 917 - 935, August 1988.

[2] B. K. P. Horn and B. G. Schunck, "Determining optical flow." *Artificial Intelligence* 17 (1981) pp. 185 - 203.

[3] C. Q. Shu and Y. Q. Shi, "Computation of motion from stereo image sequence using the unified optical flow field," *Proceedings of SPIE's 1990 International Symposium on Optical and Optoelectronic Applied Science and Engineering*, San Diego, CA, July 1990.

[4] C. Q. Shu and Y. Q. Shi, "Unified optical flow field," *Proceedings of the 1990 Conference on Information Sciences and Systems*, p. 445, Princeton University, NJ, March 1990.

[5] C. Q. Shu and Y. Q. Shi, "On unified optical flow field" *Pattern Recognition*, (Accepted).

[6] W. B. Thompson, "Introduction to the special issue on visual motion," *IEEE Transactions on Pattern Analysis and Machine Intelligence*, vol. 11, no. 5, pp. 499-450, May 1989.

[7] W. Richards, "Structure from stereo and motion," *J. Opt. Soc. Amer.*, vol. 2, pp. 343-349, Feb. 1985.

[8] H. C. Longuet-Higgins and K. Prazday, "The interpretation of a moving retinal image," *Proc. Roy. Soc. London Ser B* 208, 358-397 1980.

[9] C. Q. Shu and Y. Q. Shi, "A new approach to motion analysis from a sequence of stereo images," *Technical Report No. 18, Electronic Imaging Laboratory, Department of Electrical and Computer Engineering, New Jersey Institute of Technology, Newark, NJ*, 1990.

[10] C. Q. Shu and Y. Q. Shi, "Motion estimation based on a parallelogram model using unified optical flow field approach," *Technical Report No. 20, Electronic Imaging Laboratory, Department of Electrical and Computer Engineering, New Jersey Institute of Technology, Newark, NJ*, 1990.